Stability of highly supersaturated vanadium electrolyte solution and characterization of precipitated phases for Vanadium Redox Flow Battery

Waldemir Moura Carvalho, Laurent Cassayre, Delphine Quaranta, Fabien Chauvet, Ranine El Hage, Théo Tzedakis, Béatrice Biscans

Stability of highly supersaturated vanadium electrolyte solution and characterization of precipitated phases for vanadium redox flow battery

Waldemir M. Carvalho Jr, Laurent Cassayre, Delphine Quaranta, Fabien Chauvet, Ranine El-Hage, Theodore Tzedakis, Béatrice Biscans *

Laboratoire de Génie Chimique, Université de Toulouse, CNRS, INP, UPS, Toulouse, France

ARTICLE INFO

Article history:
Received 25 November 2020
Revised 26 January 2021
Accepted 27 January 2021
Available online 12 February 2021

Keywords:
Vanadium Redox Flow Batteries
Supersaturated electrolyte
Precipitation
Vanadium sulfate
Vanadium hydrates

ABSTRACT

The vanadium redox flow battery (VRFB) has been receiving great attention in recent years as one of the most viable energy storage technologies for large-scale applications. However, higher concentrations of vanadium species are required in the H_2O-H_2SO_4 electrolyte in order to improve the VRFB energy density. This might lead to unwanted precipitation of vanadium compounds, whose nature has not been accurately characterized yet. For this purpose, this study reports the preparation of $V^{(II)}$, $V^{(III)}$, $V^{(IV)}$ and $V^{(V)}$ supersaturated solutions in a 5 M H_2SO_4-H_2O electrolyte by an electrolytic method, from the only vanadium sulfate compound commercially available ($VOSO_4$). The precipitates obtained by ageing of the stirred solutions are representative of the solids that may form in a VRFB operated with such supersaturated solutions. The solid phases are identified using thermogravimetric analysis, X-ray diffraction and SEM. We report that dissolved $V^{(II)}$, $V^{(III)}$ and $V^{(IV)}$ species precipitate as crystals of VSO_4, $V_2(SO_4)_3$ and $VOSO_4$ hydrates and not in their anhydrous form; conversely $V^{(V)}$ precipitates as an amorphous V_2O_5 oxide partially hydrated. The measured hydration degrees (respectively 1.5, 9, 3 and 0.26 mol of H_2O per mol of compound) might significantly affect the overall engineering of VRFB operating with high vanadium concentrations.

1. Introduction

Due to increased energy consumption and expanded use of renewable energy sources, there is currently a great interest in large-scale energy storage systems, which can store electrical energy and release it on demand [1]. Among several candidates, the redox flow batteries (RFBs), and specifically the all-Vanadium Redox Flow Batteries (VRFB), are considered as a promising technology thanks to their i) good response rate for charge and discharge, ii) energy efficiency higher than 80% in large installations, iii) complete recycling after very high number (>10000) of cycles and (iv) flexible design [2–10]. A RFB is an electrochemical system that stores electrical energy in chemical form, in two separate electrolyte storage tanks containing different redox couples. In a typical set-up, the electrolytes flow through an electrochemical cell stack composed by several cells connected in parallel, to enable redox reactions on inert electronic collectors. The specific case of VRFB involves $V^{(V)}/V^{(IV)}$ and $V^{(III)}/V^{(II)}$ redox systems, in a mixture of water and sulfuric acid.

Although the VRFB is already on the market, its relatively low energy density (at the maximum 40 $Wh.kg^{-1}$ for around 2 $mol.L^{-1}$ of active vanadium concentration, in 3–5 $mol.L^{-1}$ H_2SO_4 solutions [11]) limits its application and consequently affects its broad market penetration. Indeed, the overall battery performance depends on the vanadium concentration, which determines the specific energy density of the battery: the electrolyte solution is, thus, one of the key components of the VRFB [12,13]. This is particularly true at extreme (cold or hot) working temperatures, since $V^{(V)}$ tends to precipitate at temperatures above 40 °C, while the $V^{(II)}$, $V^{(III)}$ and $V^{(IV)}$ aqueous compounds precipitate below 10 °C [14]. These features currently limit the battery operating temperature to the 10–40 °C range, and need to be taken into consideration for long period of storage of the electrolyte [15]. Even though it is possible to operate in a wider temperature range by employing lower vanadium salts concentrations, contents higher than 2 $mol.L^{-1}$ are desirable to maximize the energy density and reduce the electroactive material stored volume.

* Corresponding author.
E-mail address: beatrice.biscans@toulouse-inp.fr (B. Biscans).

https://doi.org/10.1016/j.jechem.2021.01.040

Consequently, an in-depth knowledge of solid–liquid reactions is required in order to rationalize and optimize the concentration of the different valences of vanadium in the VRFB electrolytes, and large research efforts have been carried out in this field. First, many solubility data have been established at various temperatures and sulfuric acid concentrations for the four vanadium valences [13,14,16–18]. Second, several works concern the evaluation of electrolyte stability, depending on sulfuric acid concentration, total vanadium concentration and temperature. These experiments are usually based on visual observation of the formation of solid precipitates on long term duration (typically more than a week), implementing the so-called static stability measurements [19–22]. Third, precipitation rates have been established by measurements of the vanadium concentration with time during precipitation of supersaturated vanadium solutions [23,24].

However, we found out that there is a lack of information concerning the exact nature of the solid phases formed upon precipitation, since most of the above-mentioned works do not provide characterization of the solids. For instance, in the in-depth study of $V^{(II)}$ and $V^{(III)}$ sulfate precipitation processes carried out by Mousa et al. [23], the nature of the precipitated vanadium(III) sulfate phase is mentioned to be $V_2(SO_4)_3{\cdot}xH_2SO_4{\cdot}yH_2O$, based on a very old study from Brierley [25], and no information is provided about the $V^{(II)}$ product. It is well established that transition metal ions usually precipitates in the form of sulfate hydrates $MSO_4.nH_2O$ in sulfuric acid media. The number of molecules of water in the hydrate structure (n) strongly depends on the concentration of H_2SO_4 and on the temperature [26], with, for instance, n = 1, 4, 5, 6 or 7 for M = $Fe^{(II)}$ [27], n = 1, 3 or 5 for M = $Cu^{(II)}$ [26] and n = 1, 4, 6, 7 for M = $Zn^{(II)}$ [28]. In the case of vanadium, it is usually admitted that $V^{(V)}$ precipitates in its oxide form V_2O_5 [29] while $V^{(IV)}$, $V^{(III)}$ and $V^{(II)}$ form sulfate salts, respectively $VOSO_4$, $V_2(SO_4)_3$ and VSO_4 [14]. Nevertheless, as illustrated by the thermodynamic analysis of the V-S-H_2O system provided by Zhou and coworkers [30], there is clearly a lack of information regarding the composition of the stable solid phases and especially the vanadium sulfate hydrates that may form in the operating conditions of VRFB. To our knowledge, the only available product characterization is provided by Wen et al. [31], who identified the compounds $V_2O_5.1.6H_2O$ and $V_2(SO_4)_3{\cdot}10H_2O$ by X-Ray diffraction, after precipitation at 25 °C. However, this study covers only two valences of vanadium, and the quality of the powder diffraction reference files related to vanadium sulfate hydrates is very poor, which calls for additional analyses of the products.

Within the global objective of providing a better knowledge of vanadium chemistry in high concentrated sulfuric acid solutions, the present study focuses thus on the preparation and identification of the precipitation products formed in VRFB operating conditions. Especially, the amount of structural water molecules incorporated in the solid phases constitutes a point of interest, since it may help to better estimates the influence of solid phase formation on the overall VRFB operation. We report here (i) the preparation of $V^{(II)}$, $V^{(III)}$, $V^{(IV)}$ and $V^{(V)}$ supersaturated electrolytes by electrolytic synthesis, (ii) the quantitative monitoring of the precipitation in stirred solutions and (iii) the characterization of the solid precipitates by complementary methods (microscopic observations, X-ray diffraction and thermogravimetric analysis).

2. Materials and methods

2.1. Preparation of vanadium supersaturated electrolytes

The principle of preparation of vanadium supersaturated solutions relies on the electrolytic dissolution of a $V^{(IV)}$ powder. Electrolytic oxidation or reduction of the solution has been carried out in an electrolytic cell which consists of two compartments separated by an ion-exchange membrane. The solute slowly dissolves in the solvent and is simultaneously converted to another oxidation state, thereby increasing the overall concentration of the solution. This method enables to produce supersaturated solutions for each valence separately, with a high degree of supersaturation.

The various redox valences of vanadium have been prepared from a $VOSO_4.nH_2O$ (99.9% purity) commercial salt supplied by Alfa Aesar. The $VOSO_4.nH_2O$ commercial powder was analyzed by thermogravimetric analysis (TGA) and inductively coupled plasma optical emission spectroscopy (ICP-OES), and the number of water molecules (structural water and free water) was found to be 4.4. The electrolyte was composed of 5 mol.L^{-1} sulfuric acid solution (H_2SO_4, 96%, Carlo Erba) and ultrapure water (18.2 MΩ.cm). A high sulfate concentration was chosen in order to decrease the solubility of the sulfate compounds thanks to the so-called "common ion effect". As a result, high degree of supersaturation and acceptable precipitation rates were obtained. Even if the chosen H_2SO_4 concentration (5 mol.L^{-1}) is higher than the commonly used concentration in VRFB (3 mol.L-1), it was chosen as a limit value to obtain larger amounts of precipitates and provide a quantitative analysis on the hydration degrees of the precipitates.

A half-cell configuration was implemented to carry out the electrosynthesis: each electronic reaction (oxidation or reduction of a vanadium solution) was performed in the working electrode compartment, while solvent decomposition occurred in the counter electrode compartment. The electrolytic reduction or oxidation of the commercial $VOSO_4$ $4.4H_2O$ powder enabled to prepare supersaturated solutions of $V^{(III)}$ and $V^{(V)}$, respectively. The initial total amount of vanadium engaged in the experiments was equivalent to 3.15 mol.L^{-1}. Then, the obtained $V^{(III)}$ solid phase (see Section 2.2) was further used to prepare: i) $V^{(II)}$ supersaturated solutions by electrolytic reduction under inert atmosphere (1 bar of N_2), and ii) $V^{(IV)}$ supersaturated solutions by electrolytic oxidation.

All electrosyntheses were performed in a glass-made, thermoregulated electrochemical cell divided in two compartments, shown schematically in Fig. 1a. The electrodes were made of 5 mm thick bands of a 3D graphite felt, having an immersed geometric surface of about 5 cm^2. A Nafion cationic membrane was used as ionic separator between the two electrolytic solutions.

Electrolysis was performed under constant temperature (27 °C) and current (1 A, thus a current density of about 0.2 A.cm^{-2}) and agitation (magnetic bar at 400 rpm).

During the runs, aliquots of the electrolyte were taken at regular time intervals, using a syringe filter (0.2 μm PTFE). The vanadium concentration was determined by UV–vis spectroscopy for $V^{(IV)}$, $V^{(III)}$ and $V^{(II)}$ and by potentiometric redox titration for $V^{(V)}$ (see section 2.3 for analytical methods).

2.2. Aging and precipitation of vanadium supersaturated electrolyte

After electrolytic preparation, the four types of vanadium electrolytes were transferred into 100 mL double jacket glass reactors and kept closed at constant temperature and agitation (400 rpm) (Fig. 1b). The reactor containing $V^{(II)}$ was flushed with nitrogen gas before closing. The $V^{(IV)}$, $V^{(III)}$ and $V^{(II)}$ electrolytes aging tests were conducted at two temperatures (10 and 30 °C) while the $V^{(V)}$ electrolyte solution was maintained at 30 and 60 °C (higher temperatures were applied in order to activate the precipitation reactions).

Similar to the electrolytic preparation step, the vanadium concentrations were followed by UV–vis spectroscopy or potentiometric redox titration. The time needed for precipitation and the evolution of vanadium concentration in the solution were recorded for the four valences. After several days, the solutions were filtered on a Büchner filter with a vacuum pump and the solid phases were

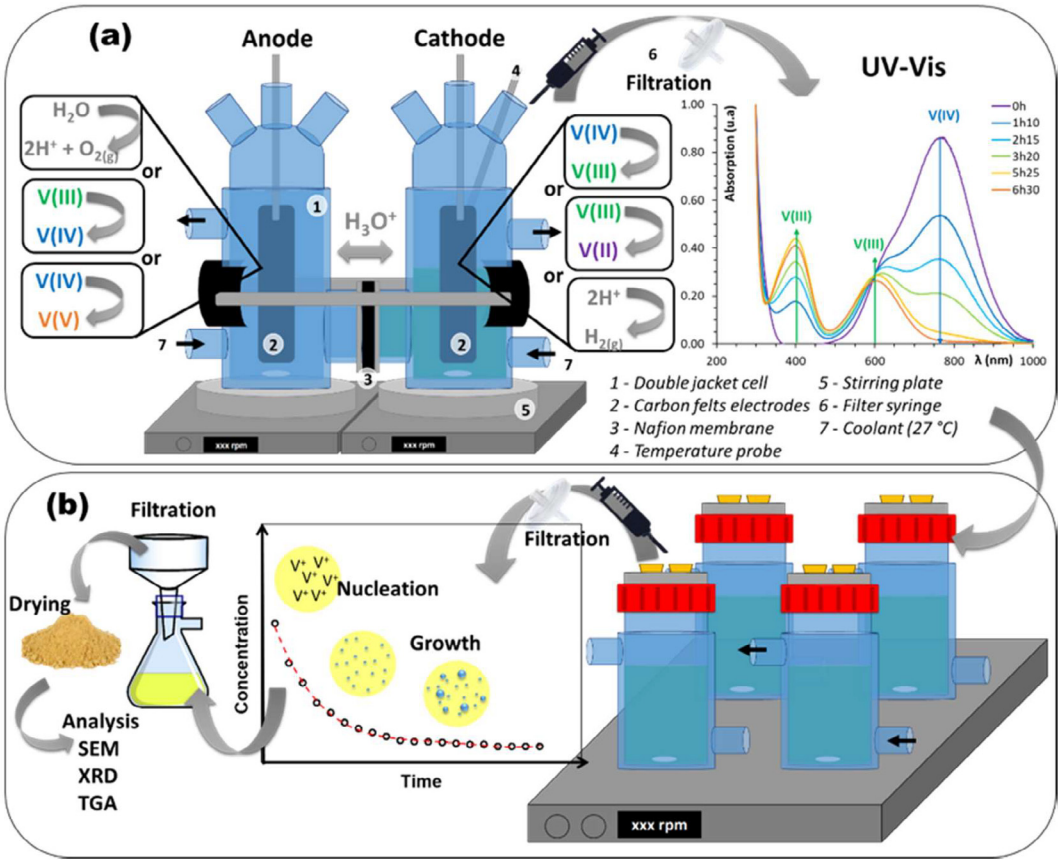

Fig. 1. Schematic representation of the overall procedure of the preparation of the four valences of vanadium sulfate salts. (a) Electrolytic preparation in a two-compartments electrolytic cell coupled with spectroscopic analysis. (b) Aging/precipitation of the vanadium supersaturated solutions in stirred and thermoregulated vessels and filtration and drying of the precipitates.

washed with ethanol 99% (vanadium compounds are soluble in water), and then dried in an oven at 60 °C for about 10 h and finally stored in a desiccator. In order to prevent oxidation, the $V^{(II)}$ precipitates were dried in a specific glass container place in the oven, under nitrogen flux.

2.3. Vanadium concentration measurements

The concentrations of the $V^{(IV)}$, $V^{(III)}$ and $V^{(II)}$ electrolytes were determined by UV–visible spectroscopy, in a wavelength range from 300 to 1000 nm, using an Agilent Cary 60 UV–Visible spectrophotometer and 1 cm thick quartz cuvettes. The electrolyte samples were filtrated with a 0.2 μm PTFE syringe filter and immediately diluted to concentrations below 0.10 $mol.L^{-1}$. The analytical procedure, adapted from previous works [32,33], is fully described in the support information, including: monitoring of UV–vis spectra (Fig. S1), verification of matrix effects (Fig. S2) and calibration curves (Fig. S3) established by dissolution of known amounts of the solids prepared in this study. The following wavelengths were selected: 855 nm for $V^{(II)}$, 398 nm for $V^{(III)}$ and 766 nm for $V^{(IV)}$. Despite several trials and parameters changes, it was not possible to observe the peak at 390 nm reported by Kim and coworkers [32] for $V^{(V)}$ solution (Fig. S1d). Thus, to determine $V^{(V)}$ concentration, a potentiometric titration by the Mohr salt (Sigma Aldrich), was performed according to the reaction (1).

$$VO_2^+ + 2H^+ + Fe^{2+} \rightarrow VO^{2+} + Fe^{3+} + H_2O \quad (1)$$

The titrator was a Metrohm 702 SM Titrino autoburette and a combined Pt-Ag/AgCl/Cl^- electrode, and the solution potential was recorded thanks to the TIAMO software (Metrohm). The solution containing 0.01 $mol.L^{-1}$ of Mohr salt was prepared in 0.1 $mol.L^{-1}$ H_2SO_4, according to the protocol described in [34]. The method was verified by titration of $V^{(V)}$ solutions at different concentrations.

For both methods, preliminary ICP-OES (inductively coupled plasma optical emission spectroscopy) analysis was carried out with an ULTIMA 2 ICP-OES, providing the total vanadium concentration in the samples. These additional analyses enabled to validate the protocol.

2.4. Solid phases characterization methods

For all precipitates, X-ray diffraction (XRD) patterns were recorded on a Discover D8-2 Bruker X-Ray Diffractometer equipped with a source of Cu $K\alpha 1$ and $K\alpha 2$ radiation at a step width of 0.02 and 5 seconds per step. The morphologies and structures of the vanadium precipitates were observed with a Tabletop scanning electron microscopy (SEM) HITACHI, TM3000. Thermogravimetric analysis (TGA) was carried out on a Mettler Toledo DSC1/TGA State from 25 to 620 °C at a heating rate of 1.5 $°C.min^{-1}$ under nitrogen atmosphere up to 350 °C (for full dehydration of the compounds) and under air between 350 and 620 °C (for full oxidation of the compounds). The samples were placed in a 30 μL platinum crucible.

3. Results and discussion

3.1. Supersaturated vanadium electrolyte synthesis

Fig. 2 shows as an example the evolution of the concentration of $V^{(III)}$, $V^{(IV)}$ and total vanadium during the electrolytic reduction of a

suspension of $V^{(IV)}$ ($VOSO_4$ $4.4H_2O$ commercial powder) to $V^{(III)}$ in 50 mL of 5 mol.L^{-1} H_2SO_4 at 27 °C with stirring at 400 rpm. At the beginning of the experiment the concentration of $V^{(IV)}$ is 1.75 mol.L^{-1}, which is slightly higher than the reported solubility at 30 °C in 5 mol.L^{-1} H_2SO_4 solution (around 1.2 mol.L^{-1}, according to [18]). As electrolysis is running, VO^{2+} ions are consumed, leading to a full dissolution of the suspension and a homogeneous solution. The total concentration of vanadium increases from approximately 1.8 to 3.0 mol.L^{-1}. This last value corresponds to the total amount of vanadium introduced in the reactor (3.15 mol.L^{-1}). Thus, even if a transfer of vanadium ions through the Nafion membrane could be expected from one half-cell to the other during electrosynthesis, the amount of transferred vanadium was small. After 7 h 30 min to 8 h, a concentration plateau is reached, for which it is considered a full vanadium conversion is obtained and the electrolysis stopped.

The highly supersaturated $V^{(III)}$ electrolyte is then transferred in the precipitation vessel in order to obtain a $V^{(III)}$ solid phase from which the $V^{(II)}$ and $V^{(IV)}$ supersaturated electrolyte are prepared.

Similar results were obtained for ($V^{(III)}$-> $V^{(II)}$) and ($V^{(III)}$->$V^{(IV)}$) conversions: the initial solution is supersaturated regarding $V^{(III)}$ solubility, so the electrolysis starts with an excess of solid. As electrolysis is running, particles are consumed, leading to a full dissolution of the suspension and a homogeneous solution with a total vanadium concentration ($V^{(III)}$ + $V^{(II)}$) and ($V^{(III)}$ + $V^{(IV)}$) equal to the initial one. Thus, we obtained in each case supersaturated solutions of respectively $V^{(II)}$, $V^{(III)}$, $V^{(IV)}$ and $V^{(V)}$ species.

The monitoring of the vanadium concentration was critical when preparing the $V^{(IV)}$ from the $V^{(III)}$ under galvanostatic conditions, because overcharging leads to undesired $V^{(V)}$ formation: the adjustment of the applied current was mandatory. This problem did not occur during $V^{(V)}$ and $V^{(II)}$ electrolyte preparation, as overcharging solely leads to $O_{2(g)}$ or $H_{2(g)}$ generation (Table 1).

For practically all the operations, a concentration plateau was reached for electrolysis durations higher than 7 h, indicating a full vanadium conversion. The time corresponding to the beginning of the concentration plateau is noted as t_{exp}. As expressed in Eq. (2), the faradic efficiency (FE) is defined as the ratio between the theoretical amount of charge required to convert a mole of vanadium and the amount of charge effectively supplied:

$$FE = \frac{z \times n_v \times F}{I \times t_{exp}} = \frac{1 \times 0.25 \times 96485}{1 \times t_{exp}} \quad (2)$$

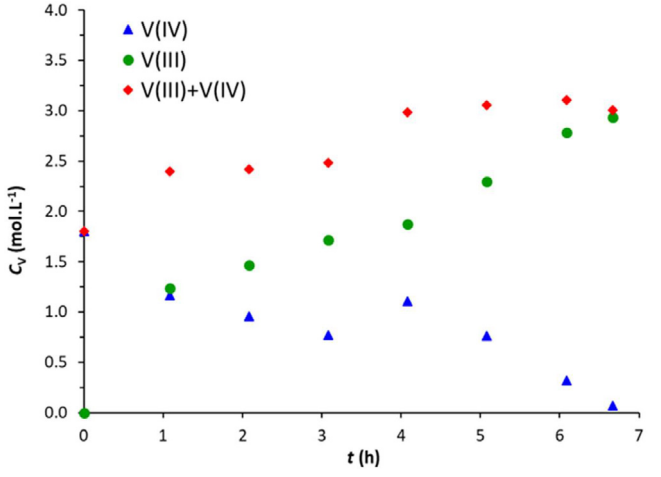

Fig. 2. Evolution of the concentrations of $V^{(IV)}$ (▲), $V^{(III)}$ (●) and total vanadium (◆) during an electrolysis at T = 27 °C by applying 1 A for 6.7 h in 50 mL of a stirred (400 rpm) suspension containing 5 mol.L^{-1} H_2SO_4 and an initial total quantity of $V^{(IV)}$ of 3.15 mol.L^{-1}.

Table 1
Summarizes the main reactions taking place in each compartment during the electrolytic preparation of the vanadium salts in sulfuric acid aqueous solutions, based on current knowledge of the aqueous vanadium speciation [19,24,30].

Conversion	Cathodic compartment	Anodic compartment
$V^{(III)} \rightarrow V^{(II)}$	$V^{3+} + e^- \rightarrow V^{2+}$	$H_2O \rightarrow 2H^+ + 0.5\ O_{2(g)} + 2e^-$
$V^{(IV)} \rightarrow V^{(III)}$	$VO^{2+} + 2H^+ + e^- \rightarrow V^{3+} + H_2O$	$H_2O \rightarrow 2H^+ + 0.5\ O_{2(g)} + 2e^-$
$V^{(III)} \rightarrow V^{(IV)}$	$2H^+ + 2\ e^- \rightarrow H_{2(g)}$	$V^{3+} + H_2O \rightarrow VO^{2+} + 2H^+ + e^-$
$V^{(IV)} \rightarrow V^{(V)}$	$2H^+ + 2\ e^- \rightarrow H_{2(g)}$	$VO^{2+} + H_2O \rightarrow VO_2^+ + 2H^+ + e^-$

*Main half electronic reactions occurring during the vanadium salts electrolytic preparation.

where n_v is the initial number of moles of vanadium (0.25 mol), z represents the number of electrons transferred (1 e^-.mol^{-1} in each conversion), F is the Faraday's constant (96485.3329C.mol^{-1}) and I is electrolysis current in ampere (1 A).

From the value of t_{exp} for each run, we deduced an average FE estimation of the conversions (1 < uncertainties $_{(\%)}$ < 4): 91% for $V^{(II)}$, 87% for $V^{(III)}$, 89% for $V^{(IV)}$ and 88% for $V^{(V)}$. The Faradaic losses are attributed i) to the partial solvent decomposition and ii) to vanadium losses through the Nafion membrane. However, due to the large surface of the electrodes (5 cm^2), the current density applied during the electrolyses is relatively low (0.2 A.cm^{-2}) and most of the supplied current was effectively used for the vanadium conversion.

3.2. Supersaturated electrolyte precipitation kinetics

The electrolyses were carried out at constant temperature (27 °C) and using an initial concentration of the vanadium starting material of 3.0 to 3.5 mol/L, except for electrolysis N° 3 carried out with 2.0 mol/L of vanadium. The aging/precipitation steps were carried out under atmospheric conditions except run N° 5 performed under nitrogen inert atmosphere Table 2.

Fig. 3 reports the temporal evolution of vanadium concentration in the supersaturated solutions of the different valence salts, during the aging/precipitation process. The initial time (t = 0) corresponds to the appearance of the first nuclei.

The initial concentrations of all the vanadium solutions are higher than the anhydrous phases solubility values reported in the literature [14,18], which confirms that each electrolytic preparation led to supersaturated vanadium solutions.

For all runs presented in Fig. 3 (at 30 and 60 °C for $V^{(V)}$, at 10 and 30 °C for $V^{(II)}$, $V^{(III)}$ and $V^{(IV)}$), the data indicate a decrease of the dissolved vanadium salt concentration and simultaneously the appearance of a solid phase. These data show two distinct precipitation behaviors. For the three lowest valences of vanadium ($V^{(II)}$, $V^{(III)}$, $V^{(IV)}$), the first precipitation sign (turbid solution and decrease of vanadium concentration) was observed rapidly (durations lower

Table 2
Summarizes the experimental conditions applied during the electrolytic preparation and aging/precipitation steps for the four valence states of the vanadium sulfate hydrated salts.

Run N°	Main redox reaction	Aging/precipitation temperature (°C)	duration(days)
1	$V^{(IV)} \rightarrow V^{(III)}$	30	1, 2 and 4
2	$V^{(IV)} \rightarrow V^{(III)}$	10	4
3	$V^{(IV)} \rightarrow V^{(III)}$	30	4
4	$V^{(IV)} \rightarrow V^{(IV)}$	30 and 60	15 and 30
5	$V^{(IV)} \rightarrow V^{(III)} \rightarrow V^{(II)}$	10 and 30	4
6	$V^{(IV)} \rightarrow V^{(III)} \rightarrow V^{(IV)}$	10 and 30	4

* Summary of the electrolyses carried out to obtain supersaturated solutions of the four valence states of the vanadium (second column), followed by their aging at various temperatures (third column), as well as the time of complete precipitation (fourth column).

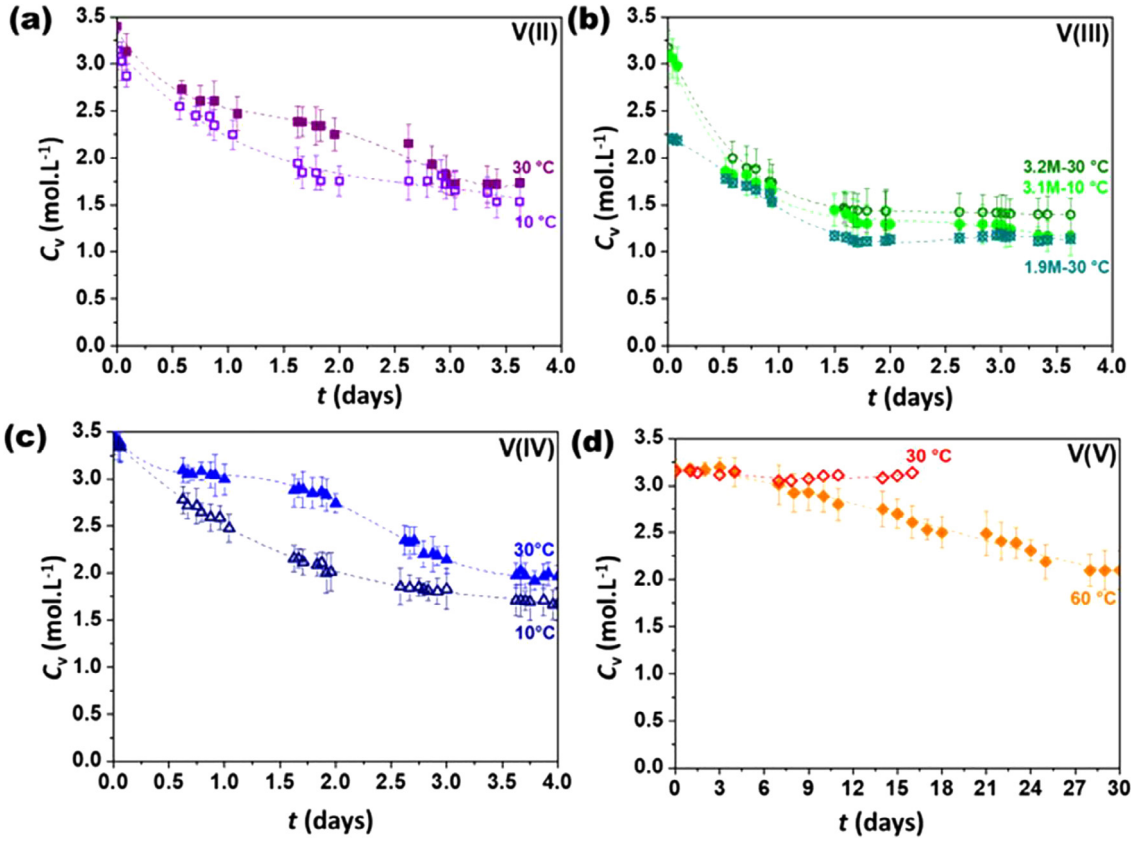

Fig. 3. Temporal evolution of the concentrations of the four valences of vanadium in supersaturated electrolytes during their aging/precipitation process at constant stirring rate (400 rpm), two different constant temperature (10 °C and 30 °C for $V^{(II)}$, $V^{(III)}$ and $V^{(IV)}$ and 30 °C and 60 °C for $V^{(V)}$) and two vanadium initial concentration for $V^{(III)}$.

than one day); then, the concentration reached a plateau after a time interval of 0.5 to 4 days (depending on the vanadium valence and temperature) and finally the system achieved an equilibrium state. After four days a significant precipitate amount was formed, which was recovered and characterized. Conversely, the concentration of the $V^{(V)}$ supersaturated solution remained stable for several days (6 to 15 days, depending on the temperature). No precipitation was observed under operating temperature of 30 °C. When carrying out the experiment at 60 °C, after 30 days, a significant precipitate amount was formed, which was recovered and characterized.

The $V^{(III)}$ solution shows a regular and classic curve towards the equilibrium plateau; conversely, the $V^{(II)}$ and $V^{(IV)}$ solutions exhibit two different slopes during the precipitation event, probably indicating the existence of a second wave of nucleation. The concentrations obtained for the different plateau, reported in Table 3, do not correspond to the solubility values mentioned in the literature for the anhydrous vanadium sulfate compounds. The values obtained in this work are generally higher, and these results will be correlated to the identified phases (Section 3.3).

Considering the temperature effect, Fig. 3 shows that temperature reduction from 30 °C to 10 °C did not affect the $V^{(III)}$ electrolyte precipitation (same concentration slope), while for $V^{(II)}$ and $V^{(IV)}$ solutions the precipitation slopes are different and goes from a two-step process to a single-step process. This behavior will be discussed thanks to the identification of the appearing phases (Section 3.3). For $V^{(V)}$ supersaturated solution, precipitation occurred only at the highest temperature (60 °C).

Mousa and Skyllas-Kazacos [23] have determined the kinetics and mechanisms for supersaturated $V^{(III)}$ and $V^{(II)}$ sulfate solutions in sulfuric acid for a range of vanadium solution compositions (1 to 3 mol.L^{-1}) and temperatures (1 °C to 20 °C). Their results showed that $V^{(III)}$ sulfate precipitates through two distinct mechanisms from diffusion control to reaction control, depending on the degree of supersaturation which was changed by changing sulfate composition. Similarly, in our study (Fig. 3b), the slopes of the kinetics curves for $V^{(III)}$ changes when changing the initial vanadium concentration from 3.2 to 1.9, which could correspond to different mechanisms due to a change of supersaturation degree. However, the comparison should take into account the nature of the

Table 3
Comparison between the significant concentration values from aging/precipitation experiments and the solubility data from the literature.

V	Temperature (°C)	Solubility (mol.L^{-1})	Initial [V^{x+}] (mol.L^{-1})	Final [V^{x+}] (mol.L^{-1})
$V^{(II)}$	10	1.06 [14]	3.13	1.56
	30	1.84 [14]	3.40	1.74
$V^{(III)}$	10	0.06 [14]	3.10	1.17
	30	0.2 [14]	3.17	1.39
	30	0.2 [14]	2.20	1.11
$V^{(IV)}$	10	0.69 [14,18]	3.41	1.67
	30	1.78 [14,18]	3.47	1.96
$V^{(V)}$	60	0.16 [14]	3.18	2.10

precipitated phases. This is why in the following section and for all the vanadium valences, we have characterized and identified the precipitated phases.

3.3. Precipitated phases characterization

3.3.1. Morphology of the precipitates

The color of the dried solid phases is dark purple, sky blue, teal green and burnt orange for $V^{(II)}$, $V^{(III)}$, $V^{(IV)}$ and $V^{(V)}$ respectively. Fig. 4 shows representative SEM micrographs of the $V^{(II)}$, $V^{(III)}$ and $V^{(IV)}$ particles after 4 days at 30 °C and those obtained from the $V^{(V)}$ electrolyte after 30 days at 60 °C. Additional micrographs obtained on salt powders prepared at 10 °C are provided in Fig. S4.

The $V^{(II)}$ powder (Fig. 4a) exhibits two main shapes, a rod-like structure of 2.7 to 11.3 μm length and polygonal structures of 5.1 to 20.8 μm length. The precipitation performed at a lower temperature (10 °C) led to an increase of the particle size, with the biggest particles reaching the centimeter scale (Fig. S4a-b). As discussed in the next sections, we attribute these two types of crystals to the presence of a mixture of V(II) and V(III) salts.

The $V^{(III)}$ precipitate (Fig. 4b) is mainly composed of polygonal structures, with some particle having a hexagonal structure of typical size ranging from 1.1 to 10.6 μm length. A lower temperature (10 °C), the particles exhibit the same morphology, while their size is slightly reduced (0.8 to 5.7 μm, see Fig. S4c). The observation of the precipitate obtained after 1, 2 and 4 days (Fig. S5) shows that the particles size increases with the precipitation time (0.5–2.5 μm, 0.7–3.0 μm and 1.1–10.6 μm for 1, 2 and 4 days) without significantly morphology change (same polygonal structures). In that case, the classical law of growth rate increasing with temperature and time is observed.

The $V^{(IV)}$ precipitates (Fig. 4c) shows similar morphology at both precipitation temperatures. It consists of big pillar structures with the agglomeration of some smaller particles (irregular structure + faceted polygon at 30 °C and only faceted polygon at 10 °C).

In the case of $V^{(V)}$ supersaturated solution, precipitated particles obtained at 60 °C show an amorphous irregular morphology (Fig. 4d). The $V^{(V)}$ precipitate is composed of particles ranging from 4.1 to 92 μm length, however, the larger particles appear to be compact agglomerates of smaller particles.

3.3.2. Crystallographic phase characterization

Fig. 5 gathers the different X-ray diffraction patterns of the precipitates obtained after 4 days of aging of the four types of vanadium electrolytes at 10, 30 or 60 °C. The $V^{(II)}$ compound XRD pattern was obtained using a closed sample holder, in a nitrogen atmosphere during the analysis in order to preserve the precipitate and prevent oxidation. The closed sample holder generated an undesired low angle scattering leading to a systematic background that was subtracted, as it was not related to the sample. All other XRD patterns are reported as obtained.

The XRD peak positions of the $V^{(II)}$ precipitated phase obtained at 10 °C or 30 °C (Fig. 5a) show Bragg reflection peaks relatively thin and well defined, which indicates a well-crystallized material. However, the XRD patterns at 10 °C and 30 °C do not overlap, showing that two different phases are probably obtained, which is in agreement with the SEM images. Furthermore, due to the poor quality of available powder diffraction files ($VSO_4.6H_2O$, $VSO_4.7H_2O$), no clear phase identification could be performed from the XRD data only.

The XRD pattern of the teal green $V^{(III)}$ precipitates (Fig. 5b) matches reasonably well with the Vanadyl (III) sulfate decahydrate

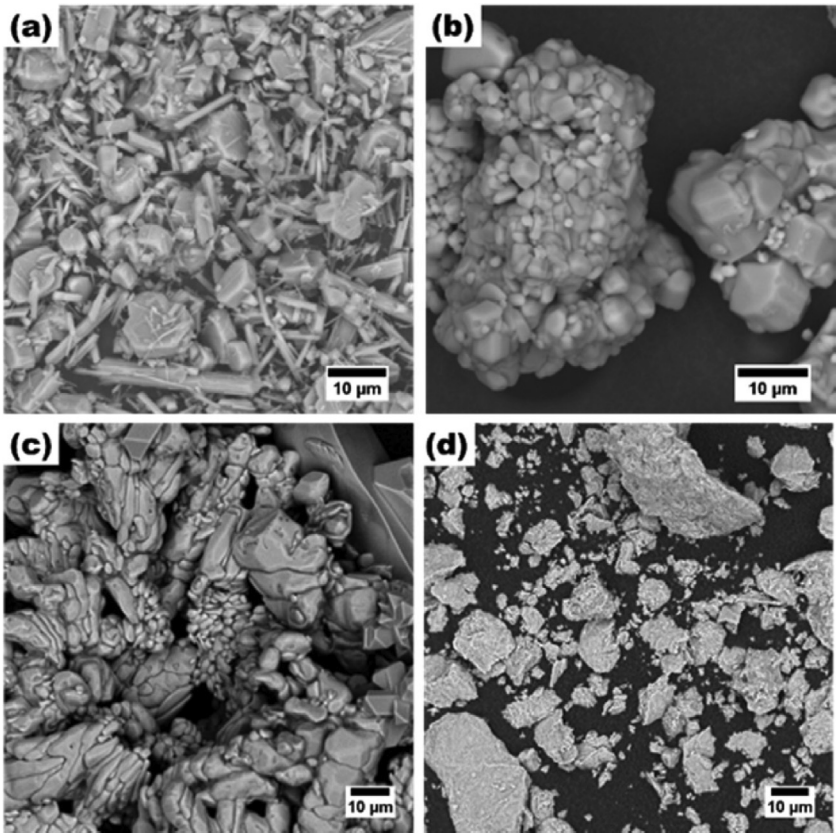

Fig. 4. SEM micrographs of the (a) $V^{(II)}$, (b) $V^{(III)}$ and (c) $V^{(IV)}$ precipitates obtained after 4 days of the 30 °C aging process, and (d) $V^{(V)}$ precipitates obtained after 30 days at the 60 °C.

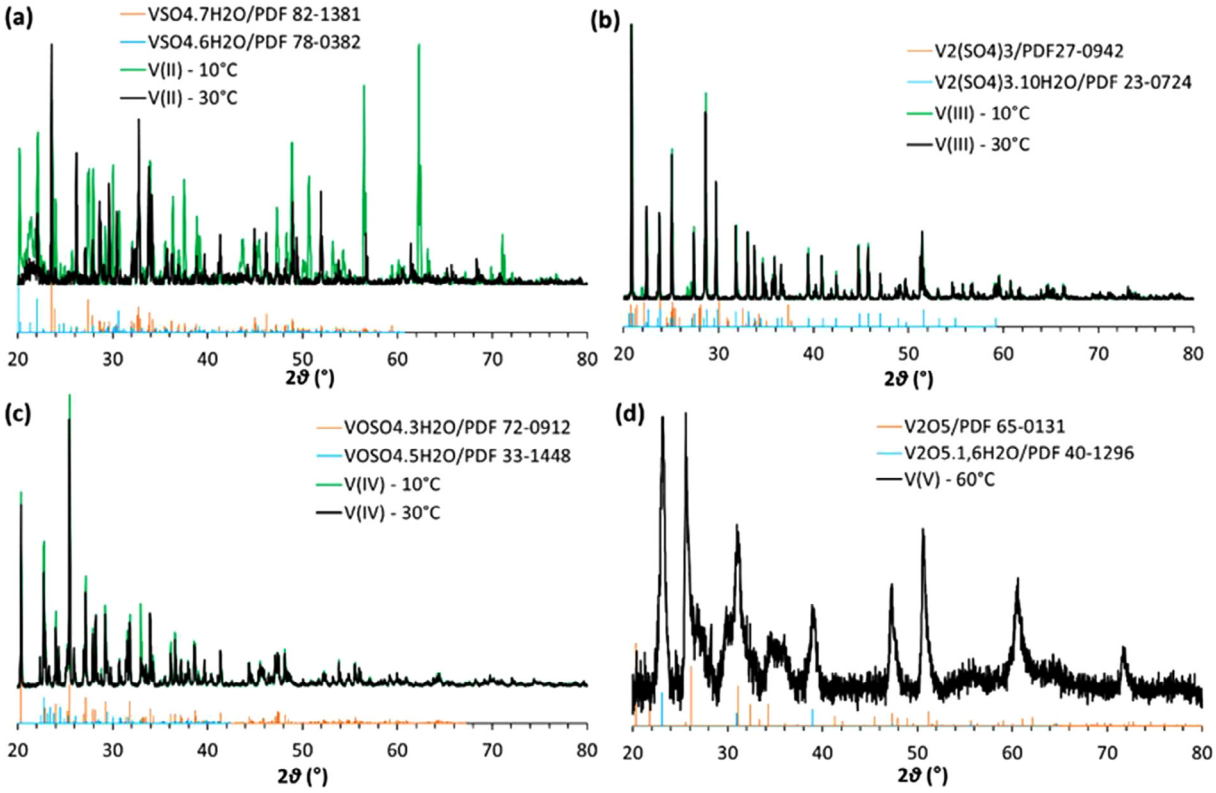

Fig. 5. X-ray diffraction patterns of the precipitated phases obtained after 4 days at 30 °C and 10 °C from (a) $V^{(II)}$, (b) $V^{(III)}$ and (c) $V^{(IV)}$ solutions; (d) after 30 days at 60 °C for $V^{(V)}$.

pattern $V_2(SO_4)_3.10H_2O$ (PDF n° 23-724) for both studied temperatures. This attribution is in accordance with XRD pattern evaluation provided by Wen et al. [31] from solid sediments recovered at negative electrode of a VRSB after operation at 25 °C. However, due to the lack of PDF files for any other $V_2(SO_4)_3$ hydrate, no better match for the $V^{(III)}$ precipitated particles can be achieved. The $V^{(III)}$ precipitation product is independent of the temperature (Fig. 5b), but also on precipitation time or vanadium concentration, with almost identical XRD patterns in all conditions as illustrated in supplementary information (Figs. S6 and S7).

The $V^{(IV)}$ precipitate XRD pattern matches the monoclinic $VOSO_4.3H_2O$ (PDF n° 72.912) (Fig. 5c). This result indicates that $V^{(IV)}$ precipitates in a different hydration degree than our commercial precursor ($VOSO_4.4.4H_2O$). Again, temperature did not influence the nature of the phase.

The XRD pattern of the dried burnt orange $V^{(V)}$ precipitate shows a broad scattered reflection at lower angles and a few broad peaks (Fig. 5d). The broad scattered reflection is a sign of amorphous materials, showing that despite the long precipitation time the $V^{(V)}$ precipitate is poorly crystallized. The broad peaks were assigned to two V_2O_5 PDF files, suggesting that $V^{(V)}$ precipitates as a mixture of the anhydrous form (PDF 65-131) and an hydrated ($1.6H_2O$ – PDF 40-1296) phase. This analysis is rather consistent with the XRD patterns provided by Wen et al. [31], which demonstrated the presence of an even less well crystallized phase, with only a few peaks attributable to the phase $V_2O_5.1.6H_2O$.

3.3.3. Thermogravimetric analysis (TGA)

The dried precipitates were characterized by TGA measurements at a heating rate of 1.5 °C min^{-1} in a nitrogen atmosphere up to 350 °C and then in air between 350 and 620 °C. The switch of atmosphere aimed at (i) dehydrating the vanadium compounds while avoiding oxidation below 350 °C, and (ii) decomposing the sulfate compounds above 350 °C into a known oxide form. The thermograms are compiled in Fig. 6.

For all vanadium compounds, the mass losses measured during the heat treatment exhibit three main steps. The mass losses up to ~ 100 °C are assigned to the volatilization of free water adsorbed to the material surface during storage. The free water content is very low (<5 wt%) for the $V^{(III)}$, $V^{(IV)}$ and $V^{(V)}$ precipitates due to efficient drying before analysis, while it is significant (about 25 wt%) for the $V^{(II)}$ compound, due to incomplete drying in nitrogen atmosphere. The masses losses above 100 °C and up to about 350 °C are assigned to structural water and account for the hydrate stoichiometry. The mass losses occurring at a higher temperature are attributed to the sulfates decomposition.

The overall mass evolution is similar for $V^{(III)}$ and $V^{(IV)}$ compounds obtained at 10 and 30 °C, which confirms XRD characterizations showing that the temperature has no influence on the nature of these precipitates (Fig. 5b and c). Similarly, there is a noticeable difference of signal during the dehydration of $V^{(II)}$ compounds obtained at 10 and 30 °C, which is also in agreement with XRD analyses that evidence two different phases (Fig. 5a).

The available amount of powder used in TGA was too small to perform XRD analysis on the remaining solid, but the homogeneous orange color of each sample enables concluding that the final compound obtained after thermal treatment at about 620 °C in air was always the same. At thermodynamic equilibrium, the phase diagram of the V-O system provided in Fig. S8 indicates that the stable phase at 600 °C in air (i.e. $\log P(O_2) = -0.67$) is V_2O_5. Therefore, the proposed decomposition reactions of the $V^{(II)}$, $V^{(III)}$ and $V^{(IV)}$ dehydrated sulfates are:

$$VSO_{4(s)} + 0.25\,O_{2(g)} \rightarrow 0.5\,V_2O_{5(s)} + SO_{2(g)} \quad (3)$$

$$V_2(SO_4)_{3(s)} \rightarrow V_2O_{5(s)} + 3\,SO_{2(g)} + 0.5\,O_{2(g)} \quad (4)$$

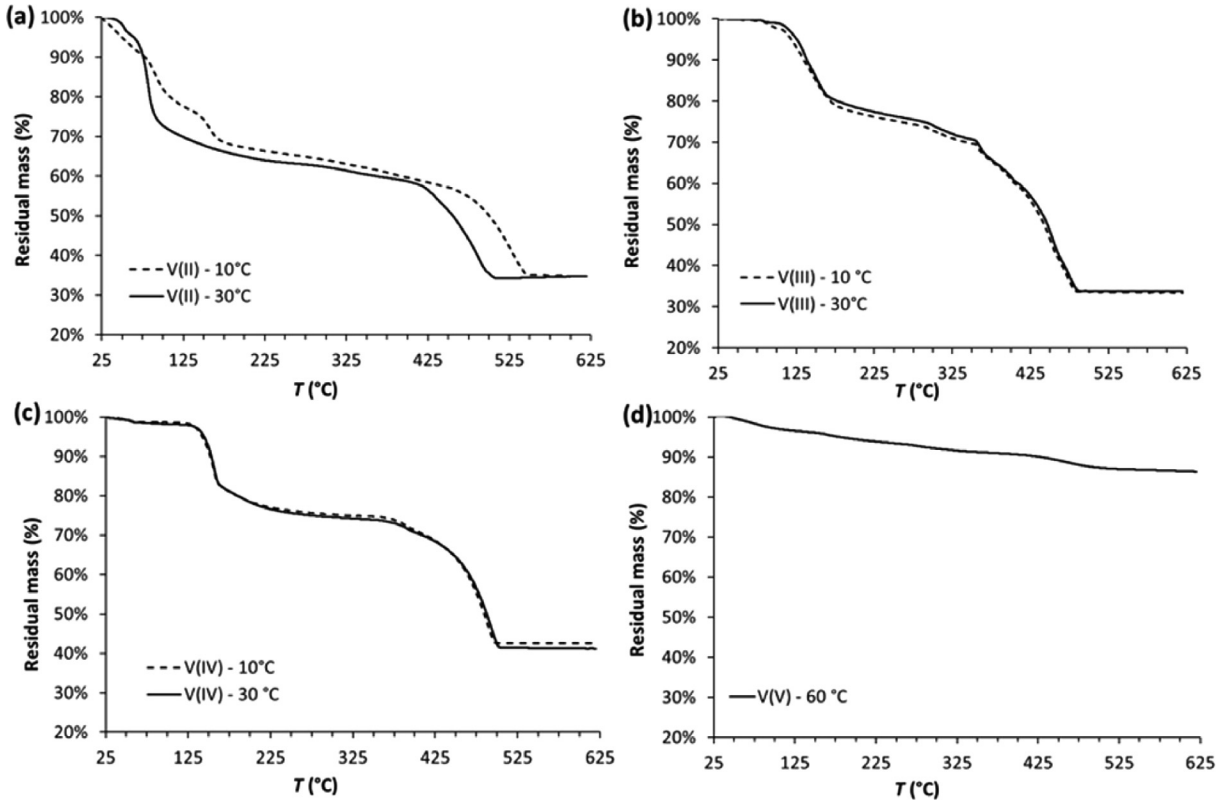

Fig. 6. Thermogravimetric analysis of the (a) $V^{(II)}$, (b) $V^{(III)}$ and (c) $V^{(IV)}$ precipitates obtained after 4 days aging process at 10 or 30 °C and (d) of the $V^{(V)}$ precipitates obtained after 30 days aging process at 60 °C.

$$VOSO_{4(s)} \rightarrow 0.5\,V_2O_{5(s)} + SO_{2(g)} + 0.25\,O_{2(g)} \quad (5)$$

Eq. (4) and Eq. (5) are similar to those proposed by Udupa [35] for the thermal decomposition of $V_2(SO_4)_{3(s)}$ and $VOSO_{4(s)}$ in air.

Table 4 reports the resulting expressions of the theoretical mass loss corresponding to the vanadium sulfates decomposition, as well as of the number of structural water molecules, based on the residual mass at 25, 100, 350 and 620 °C (m_A, m_B, m_C and m_D, respectively), and assuming that the solid products contain only one phase.

The theoretical mass losses related to sulfate decompositions (Eqs. (3) to (5)) is compared with experimental mass losses in Table 5. The relative difference between theoretical and experimental values are 7.6 ± 1.6%, 2.0 ± 0.2%, 1.1 ± 0.3% for $V^{(II)}$, $V^{(III)}$ and $V^{(IV)}$ precipitates. Furthermore, a mass loss of 4.4% is measured for $V^{(V)}$ between 350 and 620 °C, while the mass loss should be 0 (Wei et al. [36] report a full dehydration of $V_2O_5.nH_2O$ compounds at 350 °C with no further mass evolution at higher temperature).

Table 4
Expressions of (i) the number of structural water molecules x_i attributed to dehydration between 100 and 350 °C and of (ii) the theoretical mass loss Δm_{th}^{dec} attributed to sulfate decomposition into V_2O_5 in air above 350 °C.

Valence	Vanadium compound	Structural $H_2O x_i$	Sulfate decomposition Δm_{th}^{dec}
$V^{(II)}$	$VSO_4.x_{II}H_2O$	$\left[\frac{m_B}{m_C}-1\right]\times\frac{M_{VSO_4}}{M_{H_2O}}$	$m_C\left[\frac{1}{2}*\frac{M_{V_2O_5}}{M_{VSO_4}}-1\right]$
$V^{(III)}$	$V_2(SO_4)_3.x_{III}H_2O$	$\left[\frac{m_B}{m_C}-1\right]\times\frac{M_{V_2(SO_4)_3}}{M_{H_2O}}$	$m_C\left[\frac{M_{V_2O_5}}{M_{V_2(SO_4)_3}}-1\right]$
$V^{(IV)}$	$VOSO_4.x_{IV}H_2O$	$\left[\frac{m_B}{m_C}-1\right]\times\frac{M_{VOSO_4}}{M_{H_2O}}$	$m_C\left[\frac{1}{2}*\frac{M_{V_2O_5}}{M_{VOSO_4}}-1\right]$
$V^{(V)}$	$V_2O_5.x_VH_2O$	$\left[\frac{m_B}{m_C}-1\right]\times\frac{M_{V_2O_5}}{M_{H_2O}}$	0

M_i is the molar masses of compound i; m_A, m_B, m_C and m_D are respectively the residual mass measured at 25, 100, 350 and 620 °C.

The very good match between theoretical and experimental mass variations for the decomposition of $V^{(III)}$ and $V^{(IV)}$ sulfates allows to conclude that the precipitates correspond to the pure compounds $V_2(SO_4)_3.x_{III}H_2O$ and $VOSO_4.x_{IV}H_2O$. According to the expressions reported in Table 4, the hydration of the $V^{(III)}$ and $V^{(IV)}$ precipitates are respectively x_{III} = 9.0 ± 0.6 and x_{IV} = 2.8 ± 0.2, and the complete chemical formulae of the compounds comes thus to $V_2(SO_4)_3.9H_2O$ and $VOSO_4.3H_2O$. This latter composition confirms the XRD pattern attributed to the monoclinic $VOSO_4.3H_2O$ phase (PDF n° 72.912) (Fig. 5c). For $V^{(III)}$, the slight discrepancy between XRD (x_{III} = 10) and TGA (x_{III} = 9) is attributed to the poor quality of PDF files related to vanadium(III) sulfate hydrates.

On the other hand, the significant difference between theoretical and experimental mass losses corresponding to $V^{(II)}$ and $V^{(V)}$ sulfates decomposition is most likely due to the presence of additional compounds in the precipitates. Given the electrolytic method we applied for the preparation of the supersaturated solutions, we estimate that the $V^{(II)}$ compound is mixed with some residual $V^{(III)}$, while $V^{(V)}$ contains some $V^{(IV)}$. This can be explained by an incomplete electrochemical conversion, and, in the case of $V^{(II)}$, by a partial re-oxidation into $V^{(III)}$ during precipitation/aging despite the N_2 atmosphere. Based on this assumption, the purity of $V^{(II)}$ and $V^{(V)}$ (P_{II} and P_V) were determined from the decomposition step according to Eqs. (6) and (7):

$$P_{II} = \frac{M_{V_2O_5}\times\frac{m_C}{m_D} - M_{V_2(SO_4)_3}}{M_{V_2O_5}\times\frac{m_C}{2\times m_D} - M_{V_2(SO_4)_3} + M_{VSO_4}} \quad (6)$$

with P_{II} defined as the molar fraction of VSO_4 in the solid phase ($P_{II} = \frac{n_{VSO_4}}{n_{VSO_4}+n_{V_2(SO_4)_3}}$)

$$P_V = \frac{M_{VOSO_4} - \frac{M_{V_2O_5}}{2}}{M_{VOSO_4} + M_{V_2O_5}\times(\frac{m_C}{m_D} - 1.5)} \quad (7)$$

Table 5
Residual mass and transition temperatures measured by TGA during heat treatment of the vanadium precipitates under nitrogen atmosphere between 25 and 350 °C and under air between 350 and 620 °C.

Vanadium compound	$T_{precipitation}$ (°C)	$m_{A\ -\ 25\ °C}$ (%)	$m_{B\ -\ 100\ °C}$ (%)	$m_{C\ -\ 350\ °C}$ (%)	$m_{D\ -\ 600\ °C}$ (%)	Δm_{exp}^{dec} (%)	Δm_{th}^{dec} (%)
$VSO_4.x_{II}H_2O$	10	100%	75.0%	60.0%	35.0%	−25.0%	−22.9%
	30	100%	71.0%	59.0%	35.0%	−24.0%	−22.5%
$V_2(SO_4)_3.x_{III}H_2O$	10	100%	99.8%	69.9%	33.4%	−36.5%	−37.3%
	30	100%	99.7%	70.9%	33.8%	−37.1%	−37.9%
$VOSO_4.x_{IV}H_2O$	10	100%	98.7%	75.5%	42.5%	−33.0%	−33.4%
	30	100%	98.2%	74.4%	41.2%	−33.2%	−32.9%
$V_2O_5.x_VH_2O$	60	100%	96%	91%	87%	−4.4%	0.0%

$\Delta m_{exp}^{dec} = m_D - m_C$ and Δm_{th}^{dec} is calculated according to expressions reported in Table 4.

with P_V defined as the molar fraction of V_2O_5 in the solid phase ($P_V = \frac{n_{V_2O_5}}{n_{V_2O_5}+n_{VOSO_4}}$)

The resulting values are respectively P_{II} = 0.90 and 0.93 for $V^{(II)}$ precipitates obtained at 10 and 30 °C, and P_V = 0.90. The number of structural water molecules for VSO_4 and V_2O_5 (x_{II} and x_V) was then deduced from the mass loss between 100 and 350 °C, taking into account the presence of the residual impurities ($V_2(SO_4)_3.9H_2O$ and $VOSO_4.3H_2O$), according to Eqs. (8) and (9):

$$x_{II} = \frac{m_B - m_C}{m_C} \times \frac{\left(M_{VSO_4} + M_{V_2(SO_4)_3} \times \frac{1-P_{II}}{P_{II}}\right)}{M_{H_2O}} - 9 \times \frac{1-P_{II}}{P_{II}} \quad (8)$$

$$x_V = \frac{m_B - m_C}{m_C} \times \frac{\left(M_{V_2O_5} + M_{VOSO_4} \times \frac{1-P_V}{P_V}\right)}{M_{H_2O}} - 3 \times \frac{1-P_V}{P_V} \quad (9)$$

The resulting value for x_V is about 0.26, which leads to the overall formula $V_2O_5.0.26H_2O$, accounting for a mixture of V_2O_5 and an hydrate form. This composition and structure is comparable to the $V_2O_5.0.55H_2O$ xerogel prepared by Wei et al. [36] by dehydration of $V^{(V)}$ solutions at 120 °C.

As for x_{II}, the calculated water content is 1.63 and 1.31 for compounds prepared at 10 and 30 °C, respectively. These values are rather close and thus do not allow to account for a clear difference of composition between the two compounds, whereas XRD and TGA signals show that two different hydrates were formed. This can be attributed to the presence of $V^{(III)}$ in the precipitate, as well as to the poor quality of available powder diffraction files related to $V^{(II)}$ sulfate hydrates. Our best estimation for the $V^{(II)}$ precipitate composition finally comes to $VSO_4.1.5H_2O$.

4. Conclusions

Despite current researches aiming at understanding the vanadium salts precipitation in a VRFB, very little has been done to identify all the phases precipitated in the vanadium acidic solution used as VRFB electrolyte. This study has thus focused on (i) preparing $V^{(II)}$, $V^{(III)}$ and $V^{(V)}$ supersaturated solutions (ii) identifying the precipitation products in VRFB operating conditions, with the aim of improving the understanding of vanadate chemistry in a high concentrated sulfuric acid solution.

The $VOSO_4$ 4.4H_2O electrolytic oxidation/reduction enabled to prepare the four vanadium valences with a single state of oxidation in a solution containing 5 mol.L^{-1} H_2SO_4. The monitoring of the concentration of each vanadium valence in supersaturated solutions showed that the $V^{(II)}$, $V^{(III)}$ and $V^{(IV)}$ sulfate-hydrated-salts precipitate much faster than the $V^{(V)}$ compound. In addition, $V^{(II)}$ precipitates as large crystals reaching the centimeter scale at 10 °C, which is of importance for the hydrodynamics as it can cause significant problems in a VRFB. The precipitation behavior appears to be strongly affected by the temperature: (i) for $V^{(II)}$ and $V^{(IV)}$, the concentration evolution changes from a two step/plateau process to a single one when the temperature decreases from 30 to 10 °C; (ii) for $V^{(V)}$, a temperature of 60 °C is necessary to observe the solid formation and precipitation within less than 15 days.

Powder XRD analysis of each of the dried precipitates showed that, apart from $V^{(II)}$ precipitates obtained at 10 and 30 °C, the phases were similar for different aging/precipitation durations, temperature and vanadium supersaturation. The $V^{(II)}$, $V^{(III)}$ and $V^{(IV)}$ crystallized as hydrated sulfate salts, and the final hydration degree was determined as $VSO_4.1.5H_2O$, $V_2(SO_4)_3.9H_2O$, $VOSO_4.3H_2O$. The $V^{(V)}$ solution precipitated as an amorphous and partially hydrated oxide, $V_2O_5.0.26H_2O$.

The results provided in this work should be considered in the perspective of global VRFB engineering. Indeed, we show that significant amounts of water will be mobilized in the case of precipitation caused by vanadium supersaturation (up to 4.5 moles of water per mole of vanadium, in the case of $V^{(III)}$), which will in turn change the overall electrolyte properties (increase of acidity, viscosity, modification of solubility of other vanadium redox states, etc.).

Declaration of Competing Interest

The authors declare that they have no known competing financial interests or personal relationships that could have appeared to influence the work reported in this paper.

Acknowledgements

This work received financial support from the French National Research Agency (project ANR-17-CE05-0023). We want to thank Marie-Line de Solan-Bethmale from the Laboratoire de Génie Chimique (LGC) for the SEM analyses, and Cédric Charvillat from the Centre Interuniversitaire de Recherche et d'Ingénierie des Matériaux (CIRIMAT) for the powder XRD measurements.

Appendix A. Supplementary data

Supplementary data to this article can be found online at https://doi.org/10.1016/j.jechem.2021.01.040.

References

[1] P. Leung, X. Li, C. Ponce De León, L. Berlouis, C.T.J. Low, F.C. Walsh, RSC Adv. 2 (2012) 10125–10156.
[2] K.J. Kim, M.S. Park, Y.-J. Kim, J.H. Kim, S.X. Dou, M. Skyllas-Kazacos, J. Mat. Chem. A. 3 (2015) 16913–16933.
[3] G. Kear, A.A. Shah, F.C. Walsh, Int. J. Energy Res. 36 (2012) 1105–1120.
[4] M. Skyllas-Kazacos, G. Kazacos, G. Poon, H. Verseema, Int. J. Energy Res. 34 (2010) 182–189.
[5] P. Alotto, M. Guarnieri, F. Moro, Renew. Sustain. Energy Rev. 29 (2014) 325–335.
[6] L. Cao, M. Skyllas-Kazacos, C. Menictas, J. Noack, J. Energy Chem. 27 (2018) 1269–1291.

[7] Redox flow cell development and demonstration project, National Aeronautics and Space Administration, U.S. Dept. of Energy, 1979. https://ntrs.nasa.gov/search.jsp?R=19790016274 (accessed April 1, 2020).
[8] E. Sum, M. Skyllas-Kazacos, J. Power Sources. 15 (1985) 179–190.
[9] E. Sum, M. Rychcik, M. Skyllas-kazacos, J. Power Sources. 16 (1985) 85–95.
[10] L. Zeng, T.S. Zhao, L. Wei, H.R. Jiang, M.C. Wu, Appl. Energy. 233–234 (2019) 622–643.
[11] M. Skyllas-Kazacos, C. Peng, M. Cheng, Electrochem. Solid-State Lett. 2 (1999) 121–122.
[12] C. Choi, S. Kim, R. Kim, Y. Choi, S. Kim, H. Jung, J.H. Yang, H.-T. Kim, Renew. Sustain. Energy Rev. 69 (2017) 263–274.
[13] M. Skyllas-Kazacos, L. Cao, M. Kazacos, N. Kausar, A. Mousa, ChemSusChem 9 (2016) 1521–1543.
[14] M. Cheng, Electrolyte optimization and studies for the vanadium redox flow battery, Master of Science thesis, University of New South Wales, 1991.
[15] M. Kazacos, M. Cheng, M. Skyllas-Kazacos, J. Appl. Electrochem. 20 (1990) 463–467.
[16] F. Rahman, Stability and properties of supersatured vanadium electrolytes for high energy density vanadium redox flow PhD thesis, The University of New South Wales Sydney, 1998.
[17] R. El Hage, F. Chauvet, B. Biscans, L. Cassayre, L. Maurice, T. Tzedakis, Chem. Eng. Sci. 199 (2019) 123–136.
[18] F. Rahman, M. Skyllas-Kazacos, J. Power Sources. 72 (1998) 105–110.
[19] S. Xiao, L. Yu, L. Wu, L. Liu, X. Qiu, J. Xi, Electrochim. Acta. 187 (2016) 525–534.
[20] K. Wang, Y. Zhang, L. Liu, J. Xi, Z. Wu, X. Qiu, Electrochim. Acta. 259 (2018) 11–19.
[21] Y. Zhao, L. Liu, X. Qiu, J. Xi, Electrochim. Acta. 303 (2019) 21–31.
[22] M. Skyllas-Kazacos, C. Menictas, M. Kazacos, J. Electrochem. Soc. 143 (1996) L86.
[23] A. Mousa, M. Skyllas-Kazacos, ChemElectroChem. 4 (2017) 130–142.
[24] F. Rahman, M. Skyllas-Kazacos, J. Power Sources. 189 (2009) 1212–1219.
[25] J.T. Brierley, J. Chem. Soc. Trans. 49 (1886) 30–36.
[26] W. Wang, D. Zeng, X. Yin, Q. Chen, Ind. Eng. Chem. Res. 51 (2012) 5124–5134.
[27] P.M. Kobylin, H. Sippola, P.A. Taskinen, Calphad. 38 (2012) 185–193.
[28] F. Höffler, I. Müller, M. Steiger, J. Chem. Thermodyn. 116 (2018) 279–288.
[29] M. Vijayakumar, L. Li, G.L. Graff, J. Liu, H. Zhang, Z. Yang, J.Z. Hu, J. Power Sources. 196 (2011) 3669–3672.
[30] X. Zhou, C. Wei, M. Li, S. Qiu, X. Li, Hydrometallurgy 106 (2011) 104–112.
[31] Y. Wen, Y. Xu, J. Cheng, G. Cao, Y. Yang, Electrochim. Acta. 96 (2013) 268–273.
[32] N.H. Choi, S. Kwon, H. Kim, J. Electrochem. Soc. 160 (2013) A973–A979.
[33] R.P. Brooker, C.J. Bell, L.J. Bonville, H.R. Kunz, J.M. Fenton, J. Electrochem. Soc. 162 (2015) A608–A613.
[34] C. Menictas, The preparation and feasibility study of vanadium electrolytes prepared from intermediate vanadium compounds and the investigation of the kinetics for the dissolution of V_2O_5 in vanadium solution PhD thesis, University of New South Wales, 1993.
[35] M.R. Udupa, Thermochim. Acta. 51 (1981) 169–173.
[36] Q. Wei, J. Liu, W. Feng, J. Sheng, X. Tian, L. He, Q. An, L. Mai, J. Mat. Chem. A. 3 (2015) 8070–8075.